

Supplemental Materials and Methods:

Lanthanide Synthesis:

Preparation of YVO₄:Bi,RE Nanophosphors: Solutions (0.1 M) of the rare-earth (RE) dopants [Sm(NO₃)₃, Dy(NO₃)₃, Eu(NO₃)₃], Y(NO₃)₃, and Na₃VO₄ were prepared beforehand. 14.2 mg of Bi(NO₃)₃ was added into 3 mL of a 10 w/w% solution of PEG (Mn ~ 2,000). This solution was then rapidly dissolved through brief sonication before being heated to 70 °C in an oil bath under magnetic stirring. A solution of Y(NO₃)₃ (800 µL) and the RE solution (e.g., Eu(NO₃)₃) (50 µL) was premixed and then added drop-wise into the stirring PEG solution. The PEG solution instantly turned white upon addition of the Y+RE mixture. This solution was stirred for 30 minutes, followed by the drop-wise addition of the Na₃VO₄ solution (950 µL). The suspension turned yellowish at this stage and the mixture was again stirred for 30 min. The suspension was transferred into a glass vial suitable for microwave synthesis and was heated to 180 °C at 15 bar for 60 min. Upon removal from the microwave, the suspension was pure white. The material was pelleted in a 15-mL disposable centrifuge tube and the PEG supernatant was removed. The pellet was then re-suspended in 3 mL of deionized H₂O, to which was added 5 mL of a 10 w/w% PAA solution (Mn ~ 1,400). This mixture was heated back up to 70 °C and stirred for 10 min. The solution was pH adjusted to 7.5 using 5 N NaOH and stirred for an additional 30 min. The suspension was then diluted 1:10 with deionized H₂O and sonicated for 18 hours. After sonication, any larger phosphor particles were pelleted under centrifugation and the remaining translucent suspension was filtered consecutively through a 1 µm and 0.45 µm PTFE filters before being added to an ultracentrifugation filter unit for concentration and the removal of excess salts and polymers. After the entire reaction volume (~100 mL) had been passed through the membrane, the retained nanophosphors were washed 4 times with 15 mL of deionized water to exchange out the remaining solution. The final NP suspensions were white and milky in appearance and had a nanophosphor concentration of about 50 mg/mL.

Microfluidic Device Fabrication:

All photolithography masks were designed using AutoCAD (Autodesk, San Rafael, CA) and printed onto transparency film with a resolution of 30,000 dpi (FineLine Imaging, Colorado Springs, CO). To improve adhesion of subsequent photoresist layers, all wafers were first coated with a 5 µm layer of SU-8 2005 negative photoresist (Microchem Corp.) according to the manufacturer's instructions. All spin-coating steps were performed on a G3P-8 programmable spin coater (Specialty Coating Systems, Indianapolis, IN). After each coating step wafers were set on a flat surface for 10 to 20 minutes to allow photoresist to relax completely and reduce surface irregularities, except for the initial 5 µm adhesion layer of SU-8. All photoresist baking steps were done on aluminum-top hot plates (HS40A, Torrey Pines Scientific, Carlsbad CA). Mask alignment and photoresist exposure were done on a Quintel Q2001CT i-line mask aligner (Neutronix-Quintel, Morgan Hill, CA).

Bead Synthesizer Mold Fabrication

Bead Synthesizer control molds were fabricated using SU-8 2025 photoresist according to the manufacturer's instructions for creating ~ 25 µm thick channels. Flow molds were constructed with five layers of photoresist, one using AZ50 XT positive photoresist (Capitol Scientific, Austin,

TX), the other four using different types of SU-8. Layers 1 and 2 were developed separately, but layers 3-5 (all SU-8) were developed together, after they had all been exposed, as this was found to reduce bubble formation, improve height uniformity, and allow for significantly better staggered herringbone fabrication(1) After the 5th layer, layers 3-5 were developed for 6 min in SU-8 Developer, followed by hard baking for 2 hours at 165°C, with an initial ramp from 65°C to 165°C at 120°C/hr. The five layers are:

- 1) 5 µm thick SU-8 2005 layer for the high resistance push water input. Spin-coat: (1) 500rpm for 5s with 5s ramp (spread), (2) 2900rpm for 30s with 8s ramp (cast). Soft bake: 65°C 2 min/95°C 3 min/65°C 2 min. UV exposure: 7.4s at 18.4 mW/cm². Post exposure bake: 65°C 2 min/95°C 3 min/65°C 2 min. Develop: 2 min in SU-8 Developer (Microchem).
- 2) 45 µm thick AZ50 XT layer to create rounded channels at valve locations. Spin-coat: (1) 200rpm for 5s with 1s ramp (spread), (2) 1400rpm for 30s with 5s ramp (cast), (3) 3400rpm for 1s with 1s ramp (edge bead removal). Soft bake: 65°C-112°C full speed ramp for 22 min. Rehydrate overnight. UV exposure: 20s x 4 with 20s pauses in between at 18.4 mW/cm². Develop: 1:3 solution of AZ Electronic Materials AZ400k developer (Capitol Scientific). Hard bake: ramp from 65°C to 190°C at 10°C/hr, remain at 190°C for 4 hrs.
- 3) 45 µm thick SU8-2025 layer for the lanthanide inputs, mixer channel, and oil channels. Spin-coat: (1) 500rpm for 10s with 5s ramp (spread), (2) 1600rpm for 30s with 3.6s ramp (cast). Soft bake: 65°C 2 min/95°C 10 min/65°C 2 min. UV exposure: 13.1s at 18.4 mW/cm². Post-exposure: 65°C 2 min/95°C 9 min/65°C 2 min.
- 4) 30 µm thick SU8-2025 layer on top of layer 3 in the mixer channel and downstream of the T-junction. Spin-coat: (1) 500rpm for 10s with 5s ramp (spread), (2) 3500rpm for 30s with 10s ramp (cast). Soft bake: 65°C 2 min/95°C 7 min/65°C 2 min. UV exposure: 14.3s at 18.4 mW/cm². Post-exposure bake: 65°C 3 min/95°C 6 min/65°C 2 min.
- 5) 35 µm thick SU8-2025 layer on top of layer 4 on the mixing channel for the staggered herringbone grooves. Spin-coat: (1) 500rpm for 10s with 5s ramp (spread), (2) 2500rpm for 30s with 6.7s ramp (cast). Soft bake: 65°C 2 min/95°C 7 min/65°C 2 min. UV exposure: 7s at 18.8 mW/cm². Post-exposure bake: 65°C 2 min/95°C 6 min/65°C 2 min.

Imaging Device Mold Fabrication

Imaging device control molds were fabricated using SU-8 2025 according to the manufacturer's instructions for creating ~ 25 µm thick channels. Imaging device flow molds had the following layers:

- 1) ~50 µm thick layer of AZ 50 XT photoresist to create rounded channels at valve locations. Spin-coat: (1) 200 rpm for 5 s with a 1 s ramp (spread), (2) 750 rpm for 30 s with a 5 s ramp (cast), and (3) 2750 rpm for 1 s with a 1 s ramp (edge bead removal). Soft bake: 25 minutes with ramp between 65°C and 112°C at full speed, and allowed to cool to room temperature. Rehydrate overnight. UV exposure: 25 s x 3 at ~18 mW/cm². Develop: 1:3 solution of AZ AZ400k developer in water. Hard bake: Ramp from 65°C to 190°C at 10°C/hour, remaining at 190°C for 4 hours.
- 2) ~50 µm thick layer of SU-8 2050 to create all flow channels. This layer was fabricated largely according to the manufacturer's instructions, although we found that soft baking set to ramp between 65°C and 95°C (rather than simply transferring wafers between hot plates set to 65°C and 95°C) helped prevent formation of bubbles within the photoresist.

Bead Synthesizer and Imaging Device Fabrication

All molds were silanized by exposure to trichloromethylsilane (Sigma-Aldrich, St. Louis, MO) vapors for 60 minutes. Each flow mold was then coated with a 4 mm thick layer of Momentive Materials RTV 615 (R.S. Hughes, Oakland, CA) mixed at a ratio of 1:5 (cross-linker:elastomer) using a Thinky AR-250 planetary centrifugal mixer (Thinky USA Inc, Laguna Hills, CA). This 4 mm thick layer was subsequently degassed in a vacuum chamber for 60 minutes. All control molds and slides for mounting the devices were spin coated with a ~ 20 μm thick layer of RTV 615 mixed at a ratio of 1:20 via a 2 step spin process: (1) 500 rpm for 5 s with a 5 s ramp (spread), and (2) 1900 rpm for 60 s with a 15 s ramp (cast). Flow molds, control molds, and coated slides were baked at 80°C for 1 hour, 40 minutes, and 20 minutes, respectively. Following baking, PDMS flow layers were peeled from molds, cut to the appropriate size, punched with a drill press (Technical Innovations, Brazoria, TX) at inlet and outlet ports, and aligned to control layers (still remaining on the molds). The aligned devices were then baked for an additional hour before being cut from the molds, punched to create control access ports, and placed on the coated slides. The entire assembly was then baked at 80°C for 1-12 hours to finalize device bonding. Synthesis devices were mounted on regular microscope glass slides, while imaging devices were mounted on cyclic olefin copolymer slides (COP480R, Pure Slides LLC, Medford, MA) to minimize the fluorescence background.

Microfluidic Device Operation:

Valves in the microfluidic devices were actuated by 10 mm pneumatic solenoid valves (Festo Corp., Hauppauge, NY) driven by an ethernet-based, programmable fieldbus I/O system with digital output modules (750-841 Programmable Fieldbus Controller, 750-504 4-Channel Digital Output Module, Wago Corp., Germantown, WI). All fluids were injected into the microfluidic devices using pressure-driven flow from custom-made containers. Pressurized air to operate the valves and push fluids into the chips was supplied by a set of manual precision pressure regulators connected to the house air supply through a series of high efficiency filters for oil and particulate removal. A custom software platform written in MATLAB (The MathWorks Inc., Natick, MA), with a graphical user interface, allowed for real time control and script-driven automation of all aspects of the chip operation, for both the bead synthesis and imaging chips. The UV light source for droplet polymerization was a Leica EL6000 fluorescence excitation light source with a metal halide bulb and liquid light guide filtered by an Omega UV filter cube set #XF02-2 (80nm band around 330nm).

Bead Production:

All monomer-lanthanide mixtures were injected into the chip from custom-made containers using PEEK capillary tubing with an inner diameter of 65 μm and a length of 30.5 cm to provide high input resistance relative to the resistance of the staggered herringbone channel. This helps minimize any potential flow rate errors due to inaccuracies in measuring the resistance of the staggered herringbone channel or fluctuations in set pressures. On-chip resistors optimized for stable drop production at the T-junction with input pressures near the middle of the pressure regulator range were used on the oil and push water inputs. To reduce oxygen inhibition of the PEG-diacrylamide polymerization, these containers were pressurized with nitrogen (95-99% purity) supplied by a high-precision, high-speed, computer-controlled pressure regulator with

eight independent output channels (MFCS-FLEX, 8 channels, 0-1000 mBar range, Fluigent SA, Paris, France). For the same reason, the microfluidic device was surrounded by a 95-99% pure nitrogen atmosphere during operation. The high gas permeability of PDMS ensures that the interior of the microfluidic device will equilibrate with this nitrogen atmosphere (2). The compressed nitrogen for these purposes was supplied by a membrane-based nitrogen generator (Membrane Module 210, Generon IGS, Pittsburg, CA) fed from the building compressed air supply.

After polymerization, the beads were always smaller than the droplets, mostly due to oxygen-driven cross-linking inhibition on the droplet surface, and this reduction in size was highly dependent on the UV dose delivered to the droplets (the lower the dose, the smaller the beads). For the experimental conditions described here, the typical diameter shrinkage was approximately 7 μm , resulting in beads of approximately 46 μm \pm 1 μm . The measured error corresponded to approximately half a pixel in the image and thus the actual size variation of the beads is likely smaller. Sizes of beads were measured by fitting a circle to 3 user-selected points on the perimeter of the bead in a brightfield image using NIS-Elements (Nikon Instruments, Melville, NY).

Bead imaging (microfluidics):

A simple microfluidic device was designed to create an ordered linear array of beads within a narrow serpentine channel (Fig. 3A) that fits approximately 190 beads in one field of view of the microscope. "Sieve" valves positioned at the end of the serpentine channel permitted fluid flow while retaining beads, facilitating pressure-driven packing of beads within the channel and maximizing imaging throughput. Multiple output ports collected both buffer and bead wastes; fluid injection ports at either side of the device allowed flushing of the serpentine from either side to clear stuck particles. These devices are mounted on cyclic olefin polymer slides (COP480R; Pure Slides, LLC., Medford, MA) to minimize autofluorescence; the PDMS itself was not significantly autofluorescent. Device control lines were pressurized to 25 psi (for fully sealing valves) and 35 psi (for sieve valves).

Prior to loading, bead batches were washed ten times in a solution of 1x Phosphate Buffered Saline (PBS) with 0.5% Tween and twice in a solution of 1x PBS with 0.1% Tween before being diluted to a working concentration of 100-200 beads per μL in 1x PBS with 0.1% Tween. Bead solutions (\sim 25 μL) were loaded into Tygon tubing (using a 1 mL syringe), which is connected directly to the device. Buffers were stored in pressurized vials connected to the device via Tygon tubing. During serpentine loading, both bead and buffer inputs were pressurized at 3-5 psi and excess buffer was directed to the waste port. During imaging, buffer solution pressure was reduced to \sim 1 psi to relax bead packing. After imaging, the output was directed to a separate bead waste port to collect imaged beads for further use.

Bead imaging (optics):

Bead imaging was performed using a Nikon Ti microscope (Nikon Instruments, Melville, NY) with a custom built illuminator. Because the microscope objectives are not transparent to the short wavelength UV illumination required to excite the lanthanides, we used a transillumination

geometry as shown in Fig. 3. Light from a full-spectrum 300W Xenon arc lamp (Newport, Irvine, CA) was collected, reflected off a 400 nm long pass mirror (CVI Melles-Griot, Albuquerque, NM) to reject visible light, then passed through a shutter and an excitation filter wheel (Sutter Instrument Co., Novato, CA), before being focused into a 3 mm diameter deep UV liquid light guide (Newport). The excitation wheel allowed switching between UV illumination for lanthanide excitation and visible light illumination for finding beads and imaging the device during bead loading. For UV imaging, the illumination light was filtered with a 292/27 excitation filter (Semrock, Rochester, NY) paired with UG11 absorptive glass (Newport). The illumination intensity at the sample was $\sim 12.5 \text{ mW/cm}^2$. For visible light imaging we used the residual visible light reflected by the 400 nm long pass mirror, which was further filtered with a 409 nm long pass filter (Semrock), infra-red reflective mirror (Edmund Optics), and an OD 1.0 neutral density filter.

The other end of the liquid light guide was mounted on the condenser mount of a Nikon Ti microscope, where the light was collimated by a fused silica lens (Newport) and projected onto the sample. Emitted light from the sample was collected by a Plan Apo 4x/0.2NA (Nikon Instruments, Melville, NY) objective, with a UV blocking filter (Edmund Optics, Barrington, NJ) placed between the objective and the sample. Emitted light was filtered through an emission filter wheel mounted beneath the objective before being focused onto the camera. We collected an image stack consisting of six different images acquired through the following filters (all from Semrock): 482/35, 510/84, 543/22, 572/15, 615/20, and 630/92. The filters used here were chosen using a Monte Carlo optimization procedure to select filters which minimize the unmixing error. Typical exposure times were 5 seconds for the first four channels and 1 second for the last two. The camera used was an Andor DU-888 (Andor Technology, Belfast, Northern Ireland) operated in conventional readout mode at 13MHz with 2x2 binning. The microscope and camera were controlled by Micro-Manager (3).

Bead images for testing bead autofluorescence in conventional dye channels were acquired on a Nikon Ti microscope with a 10x / 0.3 Plan Fluor objective and a Coolsnap HQ2 CCD camera (Photometrics, Tucson, AZ). Illumination was from a Sutter XL lamp (Sutter Instrument Company, Novato, CA) and a Chroma 89000 filter set (Chroma Technology, Bellows Falls, VA) was used to define the excitation and emission channels. The lamp was operated at full power and the exposure time for each image was 1 second.

Linear Unmixing and Image Analysis:

All data analysis was performed with custom software written in Matlab. Reference spectra for unmixing were acquired from beads doped with a single lanthanide. These beads were spotted on quartz coverslips (to minimize background fluorescence) and an image stack was acquired as described above. The background was subtracted using a local background estimation procedure and the mean luminescence of the beads in each channel was measured. The device background spectrum was measured from a region of the microfluidic device where no beads were present. These reference spectra were then normalized so that each spectrum summed to one.

Before linear unmixing, the images of the beads in the serpentine device were corrected for camera bias and dark current by subtracting a dark image. Dark images were acquired by averaging 100 frames acquired with the same exposure times as the fluorescent images, but with the camera shutter closed. The image stack was then flat-field corrected by dividing each image by a corresponding flat-field image. Flat-field images were acquired by averaging 100 frames captured through each emission filter with white-light transmitted illumination and no sample present on the microscope. While our use of an internal standard corrected for variations in excitation intensity across the field of view, we were still sensitive to wavelength-dependent pixel response nonuniformity (4). Linear unmixing was then performed using standard least squares analysis to fit the intensity of each pixel of the measured image stack to a sum of the reference spectra times the abundance of each lanthanide (5–7). This unmixing process reduced our six-channel raw data to a four-channel image stack consisting of background fluorescence and Dy, Eu, and Sm luminescence.

We then identified beads in the unmixed image by median filtering the Eu channel and performing adaptive local thresholding. The threshold parameters were adjusted to include as many pixels as possible in each bead while maintaining separation between them. For each bead identified, we calculated the pixel by pixel ratio of Dy to Eu and Sm to Eu luminescence and recorded the median Dy/Eu and Sm/Eu luminescence ratio. To minimize the effect of wavelength-dependent pixel response nonuniformity on the CCD, we only analyzed beads within the central 300 x 300 pixels on the CCD. Because the data returned by linear unmixing were on an arbitrary scale, we used a variation of Iterative Closest Point matching to determine overall scaling factors along the Dy/Eu and Sm/Eu axes to best map the observed data to the programmed codes (8, 9). Briefly, the algorithm works as follows: an initial transformation is determined that maps the brightest bead along each axis to the highest programmed level of that lanthanide. This transformation is applied to the data and the closest programmed level to each measured bead is determined. The transformation that best matches the measured beads to their closest programmed levels is determined, and the process is iterated until convergence. To account for small systematic errors between different serpentine, we determined these scaling factors separately for each serpentine. This systematic variation was largest along the Sm/Eu dimension, and correcting it reduced the overall CV by ~0.6%. This correction was statistically significant as compared to rescaling an equal number of subsets of the data without regard to which serpentine they originated from.

The Gaussian mixture model (GMM) was fit in Matlab and standard deviation ellipses and numbers of standard deviations between points and cluster centroids were determined using the Cholesky decomposition of the covariance matrix (10). Cross-validation was performed by splitting the bead data into ten disjoint sets, training the GMM on nine, and then testing the classification accuracy on the remaining test set. This was repeated for each of the ten test sets in turn. Measurement errors were determined by replicate imaging of two different serpentine of beads. For each bead, the mean and standard deviation of five repeated measurements were calculated. The standard deviations were then grouped by lanthanide ratio and averaged to give the statistical error plotted in Fig. 5B.

Supplemental Figure Captions:

Supplemental Figure 1: Reproducibility of lanthanide nanophosphor synthesis. Each individual batch of nanophosphor suspensions were diluted 1:500 in DI water from the concentrated stock solutions. A luminescence emission spectrum (400-800 nm) was obtained using a FluoroMax-3 spectrofluorometer for all of these diluted stock solutions. The excitation was the same for all solutions (285 nm through a 3-nm slit width excitation monochromator) and the emission parameters were also held constant for all emitters (3-nm emission slit width, 1-nm increment steps, and 0.1 sec integration time at each step) with the exception of the Europium nanophosphors which, due to their brightness, had slit widths of 1 nm at both monochromators. For each emitter shown, the left column shows the emission spectra of each individual batch synthesized as a stacked plot: (A) Sm, 4 batches, (B) Dy, 3 batches, and (C) Eu, 5 batches. In the right column, the normalized emission spectra for all batches are shown as an overlay for each emitter. Typically, only one color is observed in the overlaid spectra since the high reproducibility of the batches results in several spectra that are coincident.

Supplemental Figure 2: Illustration of compatibility with commonly used visible fluors. A sample of the 1/30/12 24-code beads were imaged using a Chroma Sedat quad filter set (#89000), with a Lambda XL lamp, Coolsnap HQ2 camera, 10x / 0.3 NA objective, and 1 sec exposure time for each fluorescence channel. All four channel combinations were imaged, and the corresponding images are labeled with the excitation and emission centers of the filter sets. The 402/455 (DAPI channel) image shows weak fluorescence; the other channels show negligible fluorescence with the fluorescence in the Cy5 channel being undetectable.

Supplemental Figure 3: Scatter plots of two different batches of synthesized beads. One batch was synthesized January 9th (Set 1, red); the other was synthesized on January 30th (Set 2, blue). Both were imaged on February 15th. The Set 1 batch of beads is missing one code due to a computer error. The Set 2 beads are the same beads analyzed in the main manuscript.

Supplemental Figure 4: Comparison of programmed ratios (black) and measured code centroids and three sigma error ellipses for the Set 1 (red) and Set 2 (blue) beads.

Supplemental References:

1. Gadish N, Voldman J (2006) High-Throughput Positive-Dielectrophoretic Bioparticle Microconcentrator. *Anal Chem* 78:7870–7876.
2. Gomez-Sjoberg R, Leyrat AA, Houseman BT, Shokat K, Quake SR (2010) Biocompatibility and Reduced Drug Absorption of Sol-Gel-Treated Poly(dimethyl siloxane) for Microfluidic Cell Culture Applications. *Anal Chem* 82:8954–8960.
3. Edelstein A, Amodaj N, Hoover K, Vale R, Stuurman N (2010) in *Current Protocols in Molecular Biology* (John Wiley & Sons, Inc.). Available at: <http://dx.doi.org/10.1002/0471142727.mb1420s92>.
4. Janesick JR (2001) *Scientific Charge-Coupled Devices* (SPIE Publications). 1st Ed.
5. Tsurui H et al. (2000) Seven-color fluorescence imaging of tissue samples based on Fourier spectroscopy and singular value decomposition. *J Histochem Cytochem* 48:653–662.
6. Lansford R, Bearman G, Fraser SE (2001) Resolution of multiple green fluorescent protein color variants and dyes using two-photon microscopy and imaging spectroscopy. *J Biomed Opt* 6:311–318.
7. Zimmermann T (2005) Spectral imaging and linear unmixing in light microscopy. *Adv Biochem Eng Biotechnol* 95:245–265.
8. Besl PJ, McKay ND (1992) A Method for Registration of 3-D Shapes. *IEEE Trans Pattern Anal Mach Intell* 14:239–256.
9. Segal AV, Haehnel D, Thrun S (2009) in *Proceedings of Robotics: Science and Systems (RSS)* Available at: <http://citeseerx.ist.psu.edu/viewdoc/summary?doi=10.1.1.149.3870>.
10. Press WH, Teukolsky SA, Vetterling WT, Flannery BP (2007) *Numerical Recipes 3rd Edition: The Art of Scientific Computing* (Cambridge University Press). 3rd Ed.

Figure S1

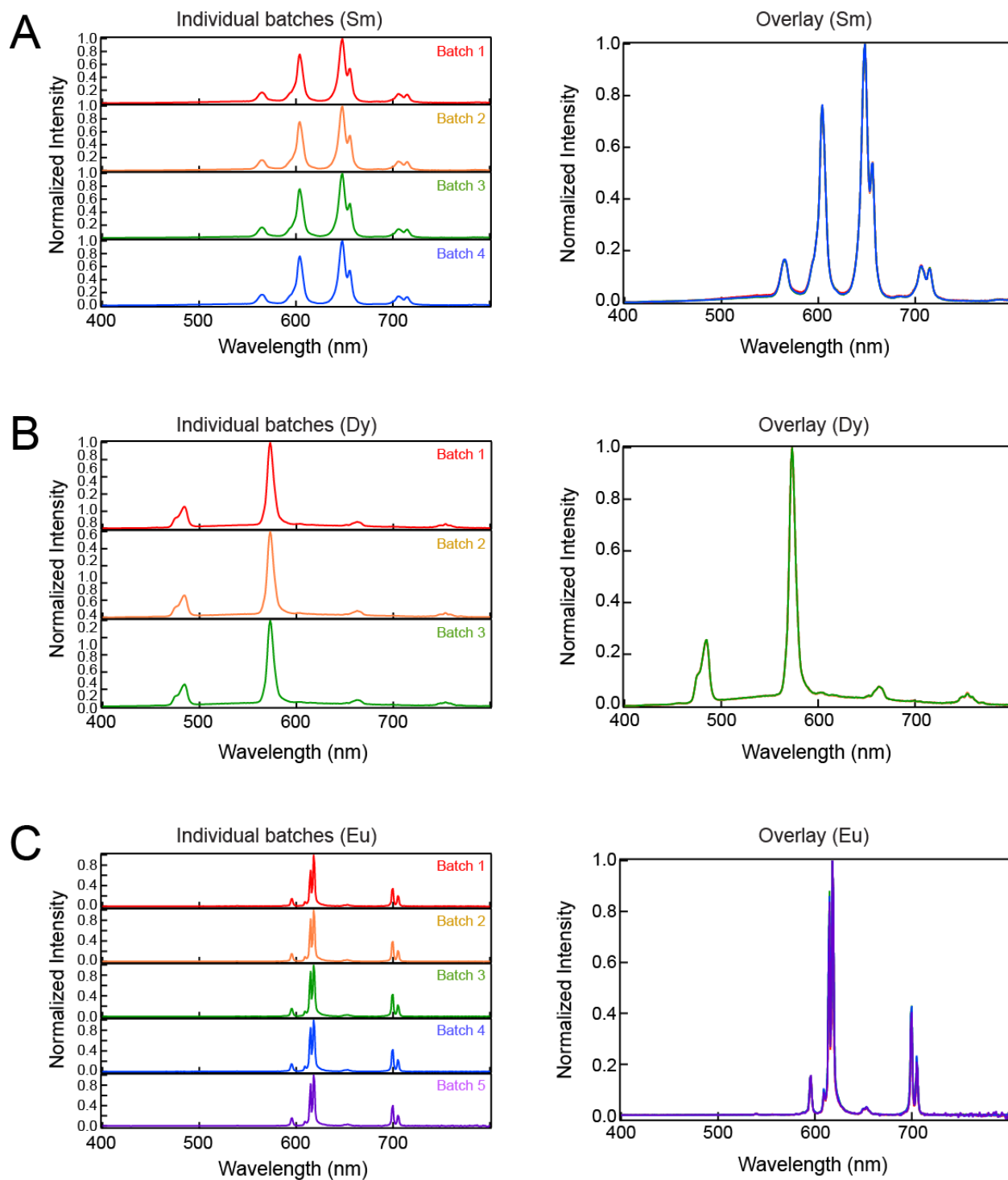


Figure S2

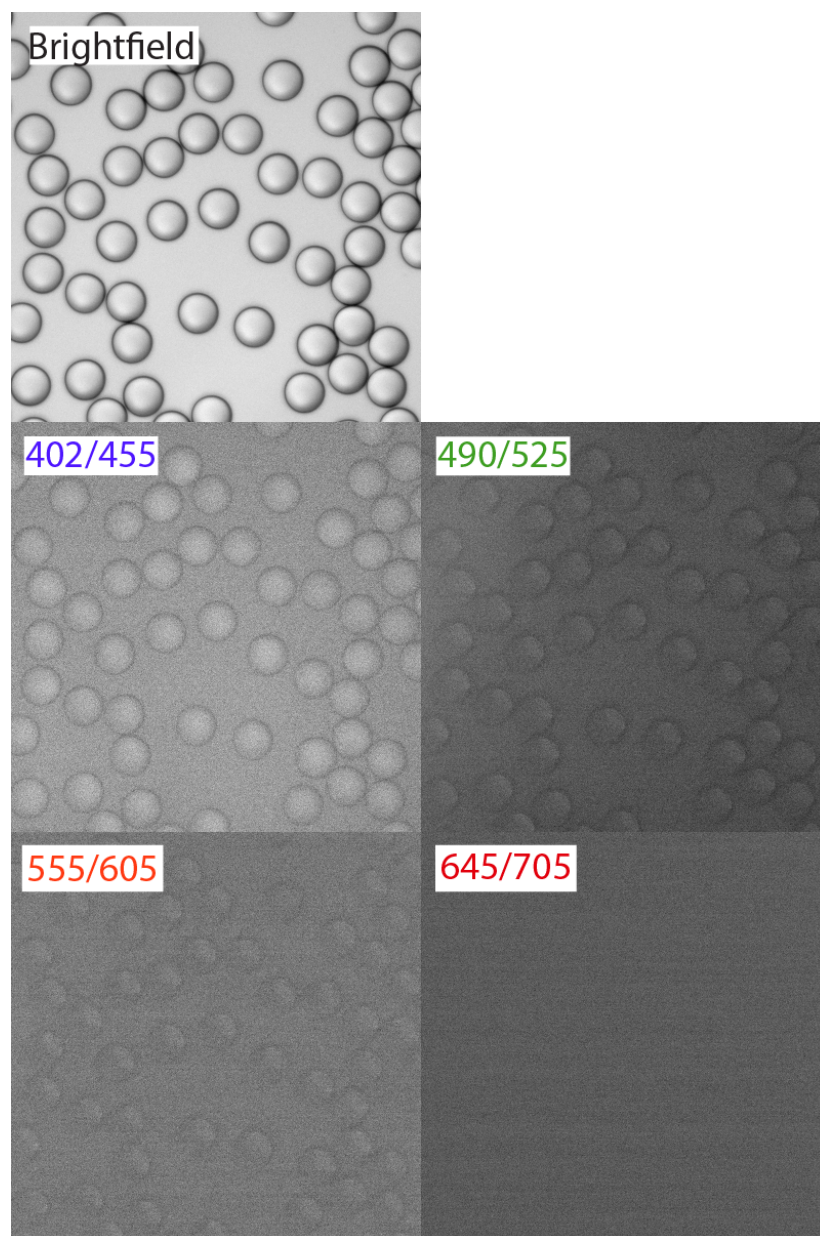


Figure S3

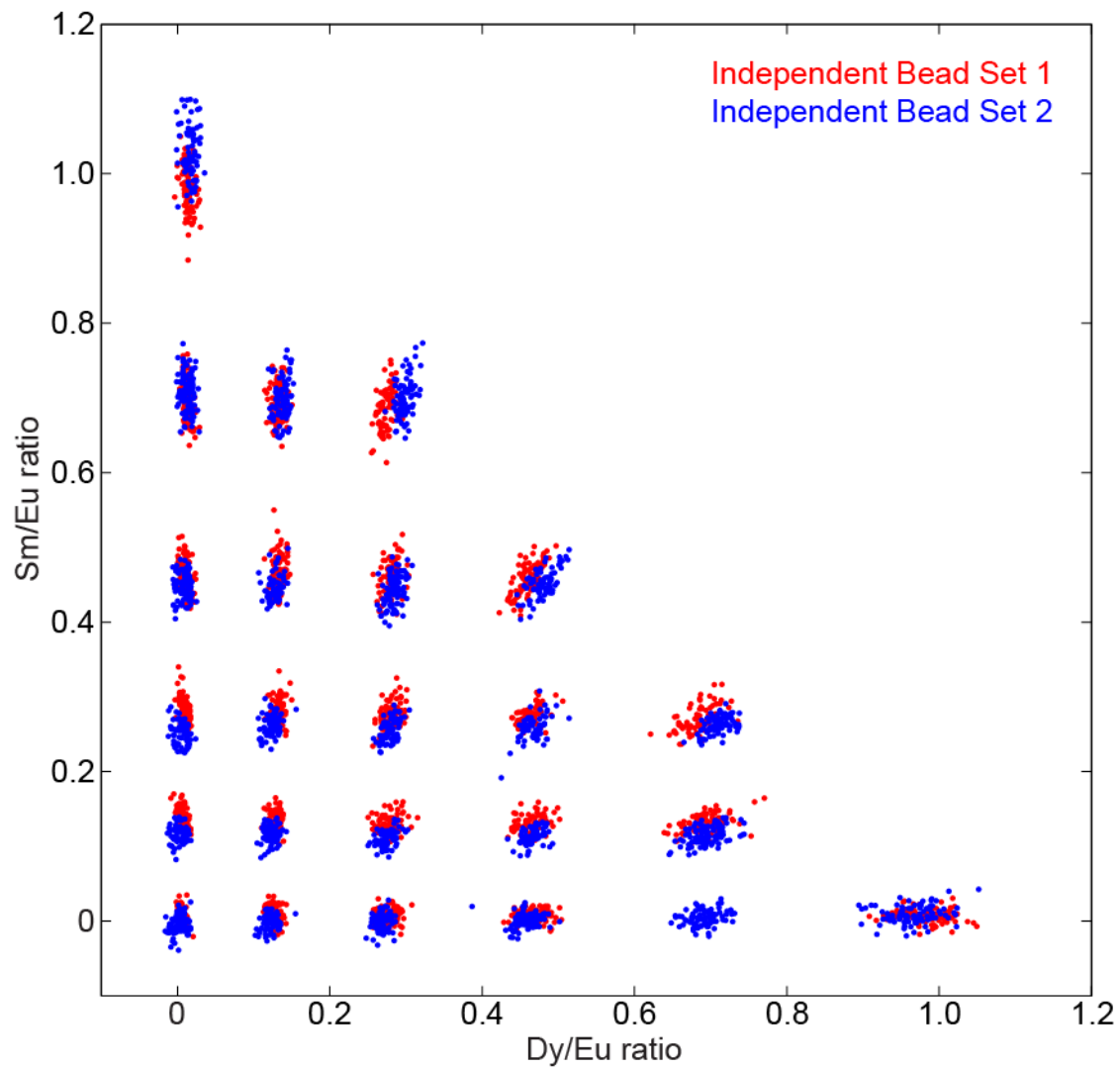


Figure S4

